



## Delayed Sahel rainfall and global seasonal cycle in a warmer climate

Michela Biasutti<sup>1</sup> and Adam H. Sobel<sup>2</sup>

Received 8 October 2009; accepted 28 October 2009; published 8 December 2009.

[1] Twenty-first century projections of global rainfall and sea surface temperature in the current generation of climate models indicate a delay in the seasonal cycle in response to increasing greenhouse gases, with important implications for the regional monsoons. In particular, the rainy season of the semi-arid African Sahel is projected to start later and become shorter. The robust agreement across models on the seasonal distribution of Sahel rainfall changes stands in contrast with large uncertainty for summertime rainfall totals there.

**Citation:** Biasutti, M., and A. H. Sobel (2009), Delayed Sahel rainfall and global seasonal cycle in a warmer climate, *Geophys. Res. Lett.*, 36, L23707, doi:10.1029/2009GL041303.

### 1. Introduction

[2] In recent decades, an increase of rainfall over the Sahel (spanning the 10N–20N band across Africa) has partially abated the drought that plagued this region from the 60's through the 80's [Nicholson, 1980; Nicholson *et al.*, 2000]. Although we understand sea surface temperature (SST) to be the proximate cause for multi-decadal variations in Sahel rainfall [Folland *et al.*, 1986; Giannini *et al.*, 2003; Hagos and Cook, 2008], there is debate regarding their ultimate cause: Is natural variability the only source of drought or did anthropogenic forcings play a role [Hoerling *et al.*, 2006; Ting *et al.*, 2009]? Are greenhouse gases (GHGs) and sulphate aerosols equally capable of affecting the Sahel [Rotstayn and Lohmann, 2002; Biasutti and Giannini, 2006]? Part of the uncertainty regarding the origin of 20th century variations derives from the vastly different model responses to GHG forcing, as seen in projections for the future [e.g., Held *et al.*, 2005; Cook and Vizi, 2006; Cook, 2008]: summer rainfall is predicted either to decrease or increase by up to 20% depending which model is used. Here we show that a robust Sahel response to GHG forcing is a seasonal redistribution of rainfall.

### 2. Delay of the Sahel Rainy Season

[3] The coupled models of the CMIP3 (Coupled Model Inter-comparison Project, phase 3) ensemble do respond coherently over the Sahel to increasing GHG forcing—not during the core of the rainy season, but during its beginning and end. Figures 1a and 1b show the 21C–20C anomalies in Sahel rainfall—the difference between the end of the 21st century (2075–2099) and the end of the 20th century (1975–1999)—as a function of calendar month, for each

model and for the ensemble mean. Across the models, rainfall anomalies are predominantly negative at the beginning of the rainy season (May and June), but positive at its end (October), indicating a delay of the main rainy season. A delay of the rains would likely induce delays in planting and—given that the time of maturity for some traditional cultivars is set by day length—a shorter growing season and a reduction in yield [Dingkuhn *et al.*, 2006]. A seasonal redistribution of rain from the beginning to the end of the rainy season occurs in all scenario simulations (Figure 1b) and in simulations forced by an exponential increase of CO<sub>2</sub> concentration (not shown). Great variability in the time at which models switch from negative to positive anomalies makes the overall change in annual mean rainfall model dependent, though anomalies at the beginning and end of the rainy season are robust. In fact, differences in the delay are largest among models previously singled out for their outlying dry (the GFDL models) and wet (the MIROC medium resolution model) projections of Sahel rainfall.

[4] The spring reduction in precipitation is not matched by a reduction in evaporation (Figure 1b): anomalous evaporation is always positive and precipitation minus evaporation (P–E) anomalies are negative for most of the year, potentially leading to drier soil. Positive evaporation anomalies independent of rainfall anomalies have been associated with anthropogenic warming in other semi-arid regions [Nicholls, 2004]. In spring, the cloudiness reduction associated with negative rainfall anomalies is not offset by higher evaporation, making surface temperatures higher than would have been otherwise. The ensemble average annual mean surface temperature over the Sahel is projected to be 3.4°C warmer, with possibly dire consequences for agriculture [Battisti and Naylor, 2009]; the projected shift in the hydrological cycle will induce even higher temperatures at the onset of the growing season, already the hottest time of the year, and drier soils when preparations for planting are necessary.

[5] We can roughly estimate changes in the beginning and end of the Sahel rainy season by interpolating from monthly data to find the dates at which rainfall becomes larger and smaller than the annual mean. The mean shifts in a middle-of-the-road scenario (A1B) are, according to this estimate, 5 and 2 days, respectively. Across scenarios (from B1, with the weakest GHG forcing, to A2, the most aggressive), the spring delay increases with increasing forcing, but the fall delay does not, indicating an increasing shortening of the rainy season. Although all scenarios show such shortening for the ensemble mean, variations across models are large, making a shortening of the rainy season a less robust projection than its delay (the model spread is shown in Figure S1 of the auxiliary material).<sup>3</sup>

<sup>1</sup>Lamont-Doherty Earth Observatory, Earth Institute at Columbia University, Palisades, New York, USA.

<sup>2</sup>Department of Applied Physics and Mathematics and Department of Earth and Environmental Sciences, Columbia University, New York, New York, USA.

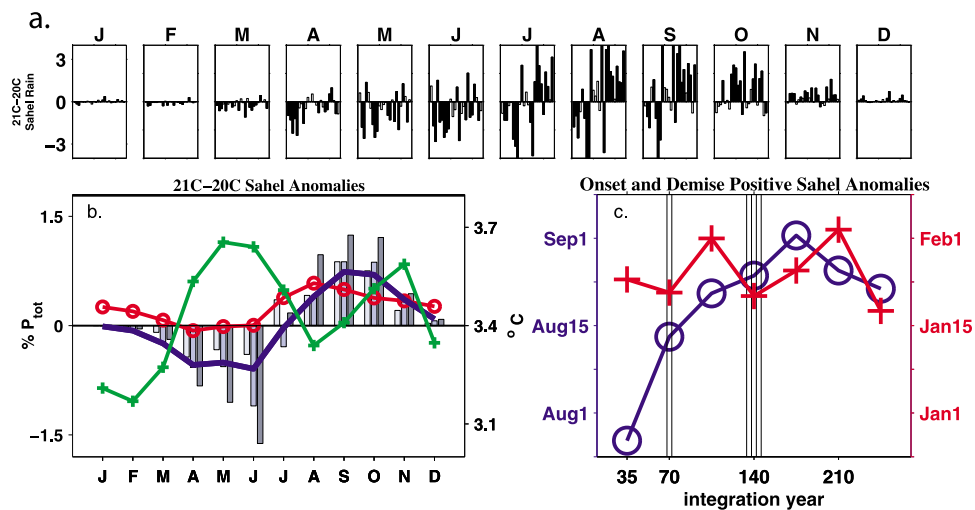


**Figure 1.** Seasonal Changes in Sahel Climate in Response to GHG Forcing. (a) Monthly (January through December) 21C-20C rainfall anomalies for individual CMIP3 models. Filled bars are significant at the 95% level. (b) Ensemble mean A1B-20C change in Sahel precipitation (solid blue), evaporation (red circles) and surface temperature (green pluses, right axis). Bars: median precipitation anomalies in three scenario with growing GHG forcing: B1-20C (light gray), A1B-20C (light blue) and A2-20C (dark gray). Only models with all scenarios are used. Precipitation and evaporation anomalies are percentages of 20C annual precipitation (left axis). (c) Dates when positive Sahel rainfall anomalies start (circles) and end (pluses) as a function of simulation year in the 1%to4X simulations. Anomalies are means over 20 years around the target dates, minus the long term mean of the control. CO<sub>2</sub> doubles at year 70, quadruples at year 140, and remains constant after that.

[6] In simulations in which CO<sub>2</sub> is the only forcing and it changes across a wide range of concentrations, the dependence of the Sahel rainy season length on the strength of the GHG forcing appears clearly. As CO<sub>2</sub> concentration grows (increasing to four times the initial values and stabilizing after that), the positive Sahel rainfall anomalies in the second half of the year start later and later but do not extend further into the dry season (Figure 1c); consequently the rainy season becomes shorter, consistent with the scenario simulations. (Changes in onset dates are the main determinant of rainy season length at interannual time scales as well [Sivakumar, 1988]).

[7] Late monsoon onsets and short rainy seasons are both problematic for agriculture [Dingkuhn *et al.*, 2006]. To begin to assess the potential impact of a shortening of the rainy season of just a few days on the people of the Sahel, we estimate changes in the distribution of the rainy season length from changes in its mean and variability. Using daily data over the periods 1981–2000 and 2081–2100 (in A1B, see also Figure S1), we estimate that the decrease in the mean length of the rainy season (of 5 days in this dataset, 2 days larger than the estimate from monthly data) and a slight (insignificant) increase in variance in the 21st century combine to make very short rainy seasons more likely in the future: what once was a one-in-ten year event, is projected to become a one-in-five year event (the change in the mean length alone would make it a one-in-six year event).

[8] Changes in Sahel rainfall seasonality occur in simulations in which GHGs are the only or the dominant forcing, but not in simulations of the 20th century (Figure S2). The latter are characterized by a year-round decrease in Sahel rainfall as the century progresses, with strongest anomalies at the core of the rainy season, consistent with observed

long-term trends. The different seasonal distribution of rainfall anomalies in simulations of the 20th and 21st century is consistent with a significant role for sulphate aerosol in forcing the 20th century decline in Sahel rainfall [Rotstayn and Lohmann, 2002; Biasutti and Giannini, 2006].

[9] The ultimate origin of the changes in the timing of the Sahel rainy season is unclear, as are the mechanics of how such changes are effected. At the same time, the sensitivity of Sahel rainfall on SST in the annual cycle [Biasutti *et al.*, 2004] and at interannual to multi-decadal time scales [Folland *et al.*, 1986; Giannini *et al.*, 2003; Biasutti *et al.*, 2008] suggests that we look at changes in SST as a potential proximate cause. Thus, in what follows we extend our investigation to the projected changes in the seasonal evolution of global SSTs, in addition to precipitation.

### 3. Delay in the Global Seasonal Cycle

[10] Global changes in the seasonal cycle of SST and rainfall are robust features of CMIP3 simulations of the next century (Figure 2). Coherent spatial patterns and temporal evolution of the seasonal cycle of global SST and precipitation are captured by empirical orthogonal functions (EOFs) and principal components (PCs) of the monthly climatology [Kutzbach, 1967]. The spatial patterns depict the changes between summer and winter (cf. the climatological August–February difference in Figure S3); the time series are nearly sinusoidal and indicate a smooth, quasi-symmetrical transition from winter to summer.

[11] Precipitation variations with an annual period are described by two EOF/PC pairs (explaining 60% and 20% of the variance in the climatology). EOF1 of precipitation (Figure 2a) captures the observed shift of rainfall to the

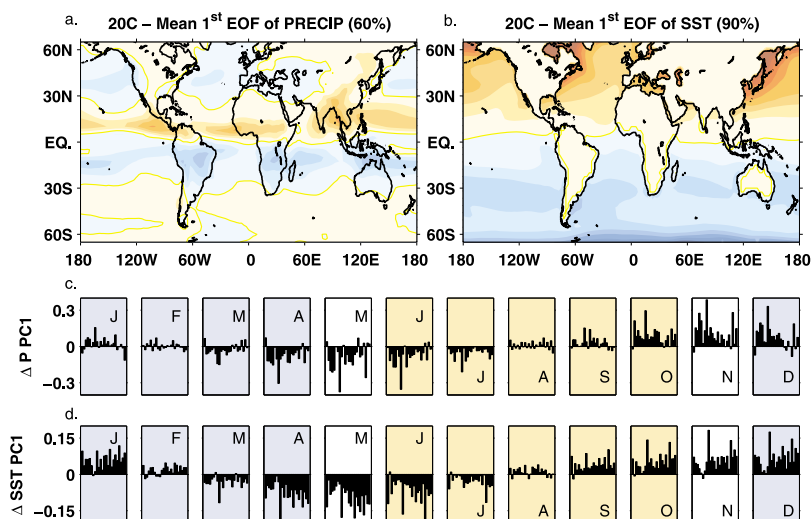


**Figure 2.** Annual Cycle of Precipitation and Sea Surface Temperature in the 20th and 21st Century. First CMIP3 ensemble mean EOF of the 20th century climatology of (a) precipitation (shading interval 1 mm/day) and (b) SST (shading interval 1°C). 21C-20C difference in PC1 of (c) precipitation and (d) SST in each calendar month and for each CMIP3 model (PC1s are normalized to unit variance). Blue and orange background shadings indicate months in which PC1 is negative or positive, no shading indicates a transition month.

summer hemisphere in the monsoon regions and in the oceanic Inter-Tropical Convergence Zone (ITCZ). The annual cycle of SST is captured by EOF1 (explaining 90% of variance, Figure 2b). It is largest at high latitudes—especially east of Asia and North America, where heat is lost to continental air in winter, and in regions of seasonal sea ice—and smaller in the tropics, where even small SST gradients can drive large changes in local circulation and precipitation [Chiang *et al.*, 2001]. The first PCs (not shown) of precipitation and temperature show a peak near August, when the northern hemisphere (NH) ocean is the warmest and precipitation reaches farthest to the North. The phase offset between SST and NH insolation is due to the high heat capacity of the ocean mixed layer; that PC1 of rainfall is equally offset underscores how strongly SST controls tropical precipitation [Biasutti *et al.*, 2004].

[12] The 21C-20C differences in PC1s (Figures 2c and 2d) are in quadrature with the PC1s themselves, indicating a small phase shift in the evolution of the seasonal cycle of both SST and rainfall during the 21st century. If we fit PC1 in 20C and 21C to sinusoids ( $\sin(\phi)$  and  $\sin(\phi - \epsilon)$ , respectively), the 21C-20C difference is approximately  $-\epsilon \cos(\phi)$  and we can quantify the shift  $\epsilon$  as 3.2 days for SST and 3.7 days for precipitation. Alternatively, the times when PC1 crosses the zero line in spring and fall provide an estimate of the delay and the change in the length of the seasons (Figure S3). On average, PC1 of SST crosses the zero line with a 4.1-day delay in spring and a 2.5-day delay in fall; for precipitation the estimates are 3.3 and 3.7 days, respectively (rainfall PC2 indicates a shift of the same order, not shown). The seasonal evolution of PC1s 21C-20C anomalies and the delay in the global annual cycle it indicates are robust across the CMIP3 ensemble. Variations in the estimates of the delay are especially small in the case of SST (Figure 2d and S4), suggesting that the difference between the delay in spring and fall might be robust and that, by this measure, the NH summer would become shorter by a day and a half. Of course, given the expected annual mean increase in

temperature, the warm season as defined by a fixed threshold will actually be longer than in the past.

[13] The global nature of the delay is not an artifact of EOF analysis. Figure 3 supports this claim using a simple method. The 21C-20C difference in SST is computed for November, then the same difference is computed for May and subtracted from the November result. If November SST warms more than May SST from the 20th to 21st century—indicating a delay in the seasonal cycle for a point in the NH—the result will be positive. This is the case for most of the NH (except the north Indian ocean and the region near the Asian coast), with the opposite holding for the Southern Hemisphere (SH, Figure 3). This diagnostic also shows a shift towards later advancement of precipitation into the NH over Africa, the tropical Americas, the Indian and Pacific oceans and, with less clarity, the maritime continent. A global delay in tropical rainfall is also consistent with similar projections for the South American monsoon [Li *et al.*, 2006; Seth *et al.*, 2009].

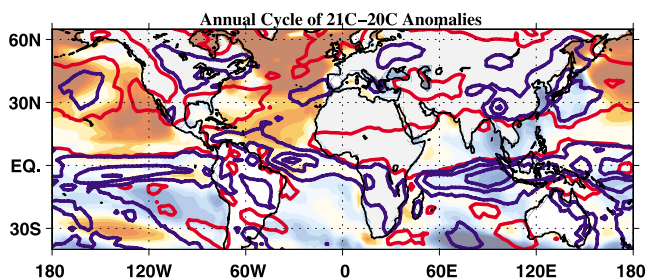


**Figure 3.** The pattern of seasonal evolution in 21C-20C anomalies. November–May (October–May) differences in SST (precipitation) 21C-20C anomalies. Precipitation is contoured (at  $[-1.5 -0.75 -0.15 0.15 0.75 1.5]$  mm/day) and SST is shaded (shading interval of 0.05°C). Warm colors and red solid contours indicate positive values; cold colors and dashed blue contours indicate negative values.

[14] The relationship between the SST and precipitation anomalies shown in Figure 3 is grossly similar to that in the annual climatology, where the largest northward SST gradients across the equator occur in summer, simultaneous with the largest poleward excursions of tropical precipitation into northern latitudes. Similar relationships linking a further northward progression of the rain band to positive northward SST gradients are also found at interannual timescales [Hastenrath, 1984; Chiang and Vimont, 2004].

[15] In particular, positive SST gradients in the tropical Atlantic are associated with a wet Sahel both in the mean seasonal cycle and at interannual time scales. We posit that the mechanisms relevant in those cases are relevant for the behavior shown in Figure 3 (i.e., both the maximum northward SST gradient and Sahel precipitation occurring later in the season in the 21st century compared to the 20th century). This suggests that the delay in the annual cycle of SST, particularly in the tropical Atlantic, may be the proximate cause of the delay in the annual cycle of rainfall in the Sahel.

#### 4. Discussion

[16] A delay in the phase of the annual cycle of high-latitude surface temperature in response to increasing GHG forcing has been modeled before and interpreted as a consequence of sea ice loss [Mann and Park, 1996]. Over sea ice, surface temperature follows local insolation with little lag. The lag increases over open water, due to the higher heat capacity of the oceanic mixed layer. The high-latitude oceans show a 21C-20C delay in the rise of surface temperature in spring and summer, but not in early fall, which is already ice-free at the end of the 20th century (not shown). This supports the idea that phase delays at high latitudes are due to sea ice loss. Recent work suggests in turn that high-latitude forcing can influence tropical climate. Modeling studies [Chiang and Bitz, 2005; Kang et al., 2009] and the paleo-record [Haug et al., 2001; Wang et al., 2008] both indicate that surface temperature changes in the North Atlantic can cause the ITCZs and the monsoons to migrate further poleward in the warmer hemisphere. By the same mechanisms, a delay in the summertime warming of the northern high latitudes would keep rainfall in the SH for longer, and a delay in the Southern Ocean would keep it to the north. In any single region, local feedbacks with the land surface might also be making the delay asymmetric, so that locally the rainy season would be shortened, as it is for the Sahel. For example, drier soils may delay the moistening of the atmosphere necessary to initiate convection: this mechanism has been invoked to explain the lengthening of the dry season in South America in response to GHG forcing [Li et al., 2006; Seth et al., 2009].

[17] In the 20th century, observed mid-latitude land surface temperatures show a significant shift towards early seasons, while the high-latitude Atlantic and Pacific show larger, but statistically insignificant, delays [Stine et al., 2009]. The observed advance over mid-latitude continents is not reproduced by the CMIP3 models. This disagreement between models and observations needs to be explained, but does not by itself invalidate our results for the 21st century. First, the delay in Sahel precipitation on which we focus is not present in long-term 20th century trends, neither in

observations, nor in the models (Figure S2), consistent with a lack of coherent phase shift in temperature over the same period. Second, we expect rainfall to be influenced by SST, especially tropical SST, and little or not at all by mid-latitude land surface temperature: it is likely that phase shifts in the former are governed by different physical processes than changes in the latter.

[18] Our results suggest that a phase shift of the annual cycle is a near-global response to GHG forcing and that the delay in Sahel rainfall is a regional manifestation of this global response. The robustness of these results contrasts with the lack of robustness in simulated summertime rainfall changes in the Sahel. This development strengthens our confidence in climate models, and may result in more useful projections of regional climate changes.

[19] **Acknowledgments.** We thank the modeling centers contributing to CMIP3, PCMDI for distributing the data, Naomi Naik for her help with the data, NOAA for financial support.

#### References

- Battisti, D., and R. L. Naylor (2009), Historical warnings of future food insecurity with unprecedented seasonal heat, *Science*, 323(5911), 240–244.
- Biasutti, M., and A. Giannini (2006), Robust Sahel drying in response to late 20th century forcings, *Geophys. Res. Lett.*, 33, L11706, doi:10.1029/2006GL026067.
- Biasutti, M., D. S. Battisti, and E. S. Sarachik (2004), Mechanisms controlling the annual cycle of precipitation in the tropical Atlantic sector in an atmospheric GCM, *J. Clim.*, 17(24), 4708–4723.
- Biasutti, M., I. M. Held, A. H. Sobel, and A. Giannini (2008), SST forcings and Sahel rainfall variability in simulations of the twentieth and twenty-first centuries, *J. Clim.*, 21(14), 3471–3486.
- Chiang, J., and C. Bitz (2005), Influence of high latitude ice cover on the marine Intertropical Convergence Zone, *Clim. Dyn.*, 25(5), 477–496.
- Chiang, J., and D. Vimont (2004), Analogous Pacific and Atlantic meridional modes of tropical atmosphere—Ocean variability, *J. Clim.*, 17(21), 4143–4158.
- Chiang, J., S. Zebiak, and M. Cane (2001), Relative roles of elevated heating and surface temperature gradients in driving anomalous surface winds over tropical oceans, *J. Atmos. Sci.*, 58, 1371–1394.
- Cook, K. (2008), Climate science: The mysteries of Sahel droughts, *Nat. Geosci.*, 1, 647–648, doi:10.1038/ingeo320.
- Cook, K., and E. K. Vizy (2006), Coupled model simulations of the West African monsoon system: 20th and 21st century simulations, *J. Clim.*, 19(15), 3681–3703, doi:10.1175/JCLI3814.1.
- Dingkuhn, M., B. Singh, B. Clerget, J. Chantereau, and B. Sultan (2006), Past, present and future criteria to breed crops for water-limited environments in West Africa, *Agric. Water Manage.*, 80(1–3), 241–261.
- Folland, C. K., T. N. Palmer, and D. Parker (1986), Sahel rainfall and worldwide sea temperature, *Nature*, 320(6063), 602–687.
- Giannini, A., R. Saravanan, and P. Chang (2003), Oceanic forcing of Sahel rainfall on interannual to interdecadal time scale, *Science*, 302(5647), 1027–1030.
- Hagos, S., and K. Cook (2008), Ocean warming and late-twentieth-century Sahel drought and recovery, *J. Clim.*, 21(15), 3797–3814.
- Hastenrath, S. (1984), Interannual variability and the annual cycle: Mechanisms of circulation and climate in the tropical Atlantic sector, *Mon. Weather Rev.*, 112(6), 1097–1107.
- Haug, G. H., K. A. Hughen, D. M. Sigman, L. C. Peterson, and U. Röhl (2001), Southward migration of the Intertropical Convergence Zone through the Holocene, *Science*, 293(5533), 1304–1308.
- Held, I. M., T. L. Delworth, J. Lu, K. L. Findell, and T. R. Knutson (2005), Simulation of Sahel drought in the 20th and 21st centuries, *Proc. Natl. Acad. Sci. U. S. A.*, 102(50), 17,891–17,896, doi:10.1073/pnas.0509057102.
- Hoerling, M., J. Hurrell, J. Eischeid, and A. Phillips (2006), Detection and attribution of 20th century northern and southern African rainfall change, *J. Clim.*, 19(16), 3989–4008, doi: 10.1175/JCLI3842.1.
- Kang, S. M., I. M. Held, D. M. W. Frierson, and M. Zhao (2009), The response of the ITCZ to extratropical thermal forcing: Idealized slab-ocean experiments with a GCM, *J. Clim.*, 21(14), 3531–3532.
- Kutzbach, J. (1967), Empirical eigenvectors of sea-level pressure, surface temperature and precipitation complexes over North America, *J. Appl. Meteorol.*, 6(5), 791–802.

- Li, W., R. Fu, and R. E. Dickinson (2006), Rainfall and its seasonality over the Amazon in the 21st century as assessed by the coupled models for the IPCC AR4, *J. Geophys. Res.*, *111*, D02111, doi:10.1029/2005JD006355.
- Mann, M. E., and J. Park (1996), Greenhouse warming and changes in the seasonal cycle of temperature: Model versus observations, *Geophys. Res. Lett.*, *23*(10), 1111–1114.
- Nicholls, N. (2004), The changing nature of Australian droughts, *Clim. Change*, *63*(3), 323–336.
- Nicholson, S. E. (1980), The nature of rainfall fluctuations in subtropical West Africa, *Mon. Weather Rev.*, *108*(4), 473–487.
- Nicholson, S. E., B. Some, and B. Kone (2000), An analysis of recent rainfall conditions in West Africa, including the rainy seasons of the 1997 El Niño and the 1998 La Niña years, *J. Clim.*, *13*(14), 2628–2640.
- Rotstayn, L. D., and U. Lohmann (2002), Tropical rainfall trends and the indirect aerosol effect, *J. Clim.*, *15*(15), 2103–2116.
- Seth, A., M. Rojas, and S. A. Rauscher (2009), CMIP3 projected changes in the annual cycle of the South American monsoon, *Clim. Change*, in press.
- Sivakumar, M. (1988), Predicting rainy season potential from the onset of rains in southern Sahelian and Sudanian climatic zones of West Africa, *Agric. For. Meteorol.*, *42*, 295–305.
- Stine, A. R., P. Huybers, and I. Y. Fung (2009), Changes in the phase of the annual cycle of surface temperature, *Nature*, *457*(7228), 435–440.
- Ting, M., Y. Kushnir, R. Seager, and C. Li (2009), Forced and internal twentieth-century SST trends in the North Atlantic, *J. Clim.*, *22*(6), 1469–1481.
- Wang, Y., H. Cheng, R. L. Edwards, X. Kong, X. Shao, S. Chen, J. Wu, X. Jiang, X. Wang, and Z. An (2008), Millennial- and orbital-scale changes in the East Asian monsoon over the past 224,000 years, *Nature*, *451*(7182), 1090–1093.

---

M. Biasutti, Lamont-Doherty Earth Observatory, Earth Institute at Columbia University, 61 Rt. 9W, Palisades, NY 10964-8000, USA. (biasutti@ldeo.columbia.edu)

A. H. Sobel, Department of Applied Physics and Mathematics, Columbia University, 500 W. 120th St., New York, NY 10027, USA. (ahs129@columbia.edu)

# Delayed Sahel Rainfall and Global Seasonal Cycle in a Warmer Climate

Michela Biasutti,<sup>1</sup> and Adam H. Sobel<sup>2</sup>

## Supplementary Material:

**Supplemental figure S1.** A comparison of observations and CMIP3 model simulations of the timing of the Sahel rainy season (estimated from daily data). Start date, end date, and length of the rainy season (top) and their standard deviations (bottom) in observations, 20C and 21C (A1B, daily data). A plus indicates the median value, the gray bar indicates the 25-to-75 percentiles and asterisks indicate the 2.5 and 97.5 percentiles. For 20C and 21C the statistics are calculated for the model ensemble (each model contributes its mean and standard deviation over 20 year periods). For observations, the standard deviation and percentiles are calculated based on interannual variations for the period 1961-1990. The 20C simulations overestimate the length of the rainy season, mostly due to their tendency to anticipate the start date (the springtime ramp up of precipitation is too gradual). The amount of variability in start date, end date and length of the rainy season is underestimate, although the observed variance is well within the range spanned by the models.

**Supplemental figure S2.** 20th century changes in Sahel rainfall show a general decline and no change in seasonality, both in observations and in the CMIP3 models. (Top) Observed long-term trend in Sahel rainfall as a function of calendar month for 2 different datasets (CRU, Hulme, 1992, and GHCN, Vose et al., 1992); (anomalies are in percent of annual total per decade, where the annual total is calculated from the GHCN dataset and the 1975-1999 period. (Bottom) Sahel rainfall anomalies in the CMIP3 models: difference between the 1975-1999 period in the 20C runs and the long term mean of the control pre-industrial runs. Anomalies that are significant at the 95% level are solid. Anomalies are in percentage of annual total (the annual total is calculated over the 1975-1999 period from each 20C integration).

**Supplemental figure S3.** The pattern of the global annual cycle is captured by the Summer-Winter differences. Shaded, is the August-February difference in SST and contoured is the July-February difference in precipitation in the ensemble mean (1975-1999 in 20C integrations); the shading interval for SST is 1°C, for precipitation the contours are  $\pm 1.5$  and  $\pm 7.5$ . Warm colors and red solid contours indicate positive values; Cold colors and dashed blue contours indicate negative values.

**Supplemental figure S4.** 21C-20C delay in the seasonal cycle of global precipitation and sea surface temperature (SST), as estimated from the timing of zero-crossing of PC1 of (a.) precipitation

and (b.) SST; green bars (lines) refer to the spring crossing, orange bar (lines) to the autumn crossing in each model in the CMIP3 archive (in the ensemble mean). Note that the y-axis has different limits in the two panels.

## References

- Hulme, M. A 1951-80 global land precipitation climatology for the evaluation of general circulation models. *Climate Dyn.* 7, 57-72 (1992).
- Vose, R. S. *et al.* The global historical climatology network: long-term monthly temperature, precipitation, sea level pressure, and station pressure data. Tech. Rep. ORNL/CDIAC-53, NDP-041, Carbon Dioxide Information Analysis Center, Oak Ridge National Laboratory, Oak Ridge, Tennessee (1992).

<sup>1</sup>Lamont-Doherty Earth Observatory of Columbia University.

<sup>2</sup>Department of Applied Physics and Mathematics and Department of Earth and Environmental Sciences, Columbia University

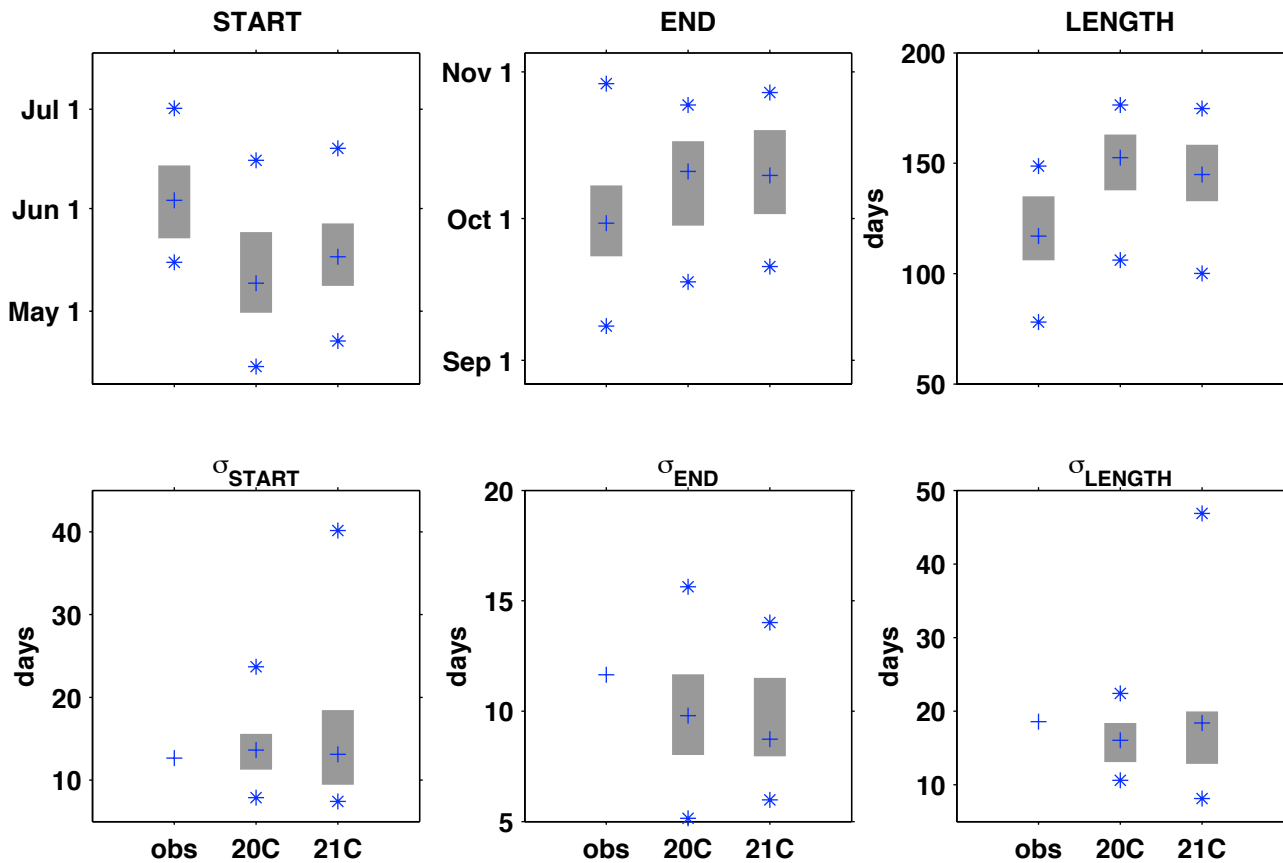


**Figure 1. Supplemental figure S1.** A comparison of observations and CMIP3 model simulations of the timing of the Sahel rainy season (estimated from daily data). Start date, end date, and length of the rainy season (top) and their standard deviations (bottom) in observations, 20C and 21C (A1B, daily data)). A plus indicates the median value, the gray bar indicates the 25-to-75 percentiles and asterisks indicate the 2.5 and 97.5 percentiles. For 20C and 21C the statistics are calculated for the model ensemble (each models contributes its mean and standard deviation over 20 year periods). For observations, the standard deviation and percentiles are calculated based on interannual variations for the period 1961-1990. The 20C simulations overestimate the length of the rainy season, mostly due to their tendency to anticipate the start date (the springtime ramp up of precipitation is too gradual). The amount of variability in start date, end date and length of the rainy season is underestimate, although the observed variance is well within the range spanned by the models.

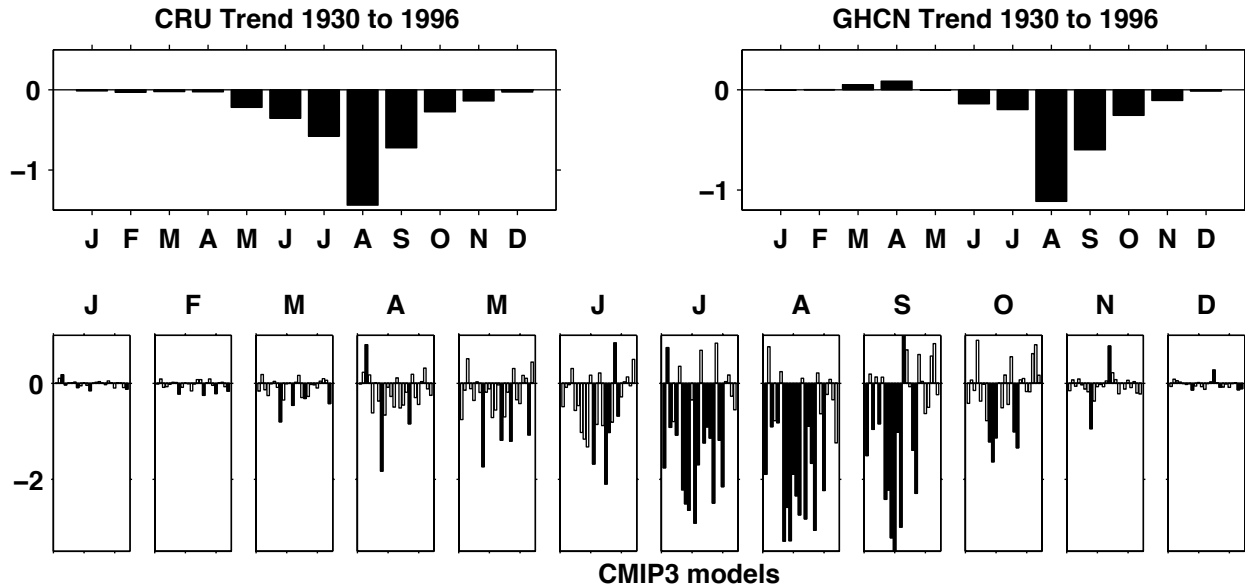


**Figure 2. Supplemental figure S2.** 20th century changes in Sahel rainfall show a general decline and no change in seasonality, both in observations and in the CMIP3 models. (Top) Observed long-term trend in Sahel rainfall as a function of calendar month for 2 different datasets (CRU, Hulme, 1992, and GHCN, Vose et al., 1992); (anomalies are in percent of annual total per decade, where the annual total is calculated from the GHCN dataset and the 1975-1999 period. (Bottom) Sahel rainfall anomalies in the CMIP3 models: difference between the 1975-1999 period in the 20C runs and the long term mean of the control pre-industrial runs. Anomalies that are significant at the 95% level are solid. Anomalies are in percentage of annual total (the annual total is calculated over the 1975-1999 period from each 20C integration).

M. Hulme. A 1951-80 global land precipitation climatology for the evaluation of general circulation models. *Climate Dyn.*, bf 7:5772, 1992.

R. S. Vose, R. L. Schmoyer, P. M. Steurer, T. C. Peterson, R. Heim, T. R. Karl, and J. Eischeid. The global historical climatology network: long-term monthly temperature, precipitation, sea level pressure, and station pressure data. *Technical Report ORNL/CDIAC-53, NDP-041*, Carbon Dioxide Information Analysis Center, Oak Ridge National Laboratory, Oak Ridge, Tennessee, 1992.

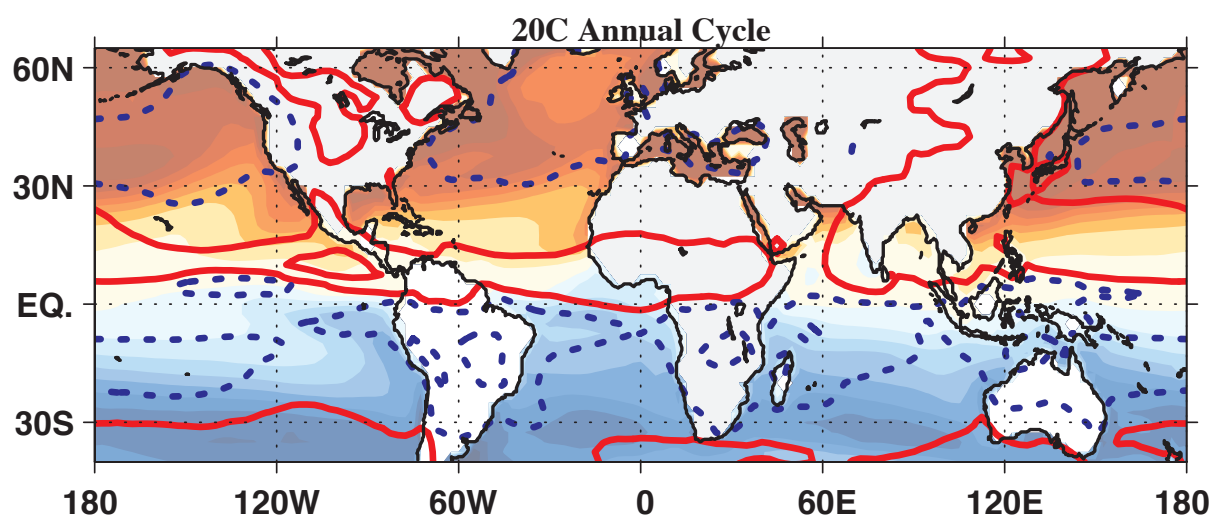


**Figure 3. Supplemental figure S3.** The pattern of the global annual cycle is captured by the Summer-Winter differences. Shaded, is the August-February difference in SST and contoured is the July-February difference in precipitation in the ensemble mean (1975-1999 in 20C integrations); the shading interval for SST is 1°C, for precipitation the contours are  $\pm 1.5$  and  $\pm 7.5$ . Warm colors and red solid contours indicate positive values; Cold colors and dashed blue contours indicate negative values.

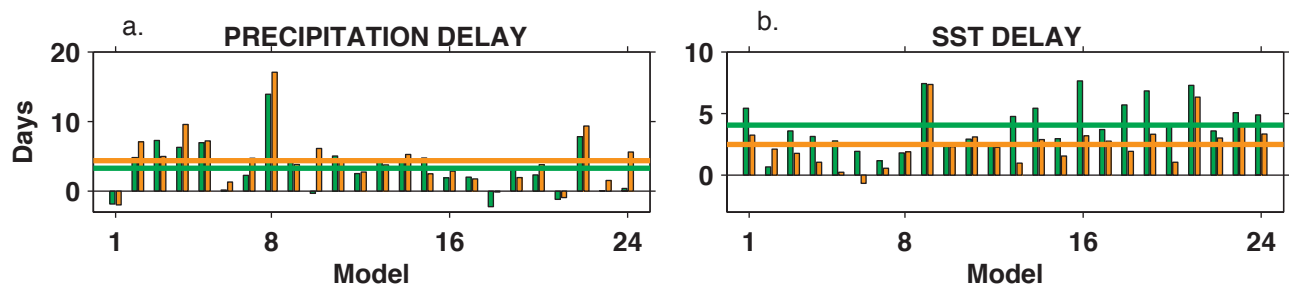


**Figure 4. Supplemental figure S4.** 21C-20C delay in the seasonal cycle of global precipitation and sea surface temperature (SST), as estimated from the timing of zero-crossing of PC1 of (a.) precipitation and (b.) SST; green bars (lines) refer to the spring crossing, orange bar (lines) to the autumn crossing in each model in the CMIP3 archive (in the ensemble mean). Note that the y-axis has different limits in the two panels.